ELSEVIER

J. Non-Newtonian Fluid Mech. 121 (2004) 1–14

Journal of Non-Newtonian Fluid Mechanics

www.elsevier.com/locate/jnnfm

Skewed Poiseuille-Couette flows of sPTT fluids in concentric annuli and channels

D.O.A. Cruz [a], F.T. Pinho [b,*]

[a] *Departamento de Engenharia Mecânica, Universidade Federal do Pará-UFPa, Campus Universitário do Guamá, 66075-900, Belém, Pará, Brazil*
[b] *Centro de Estudos de Fenómenos de Transporte, Departamento de Engenharia Mecânica, Escola de Engenharia, Universidade do Minho, Campus de Azurém, Guimarães 4800-058, Portugal*

Received 27 November 2003; received in revised form 22 December 2003

Abstract

Analytical solutions have been derived for the helical flow of PTT fluids in concentric annuli, due to inner cylinder rotation, as well as for Poiseuille flow in a channel skewed by the movement of one plate in the spanwise direction, which constitutes a simpler solution for helical flow in the limit of very thin annuli. Since the constitutive equation is a non-linear differential equation, the axial and tangential/spanwise flows are coupled in a complex way. Expressions are derived for the radial variation of the axial and tangential velocities, as well as for the three shear stresses and the two normal stresses. For engineering purposes expressions are given relating the friction factor and the torque coefficient to the Reynolds number, the Taylor number, a nondimensional number quantifying elastic effects (εDe^2) and the radius ratio. For axial dominated flows fRe and C_M are found to depend only on εDe^2 and the radius ratio, but as the strength of rotation increases both coefficients become dependent on the velocity ratio (ξ) which efficiently compacts the effects of Reynolds and Taylor numbers. Similar expressions are derived for the simpler planar case flow using adequate non-dimensional numbers.

Keywords: Phan–Thien–Tanner fluids; Helical flow; Skewed Poiseuille–Couette flow

1. Introduction

Annular flows of non-Newtonian fluids are found in a wide variety of applications: from drilling oil and gas wells and well completion operations to industrial processes involving waste fluids, synthetic fibres, foodstuffs and the extrusion of molten plastics as well as in some flows of polymer solutions. The large variety of fluids and industrial applications has been a major motivation for research in annular flow with varying degrees of complexity. An extensive bibliographic list of work on annular flows has been presented by Escudier et al. [1]. Of concern to this work are mainly previous investigations with viscoelastic fluids in concentric annuli under laminar flow conditions.

The vast majority of non-Newtonian investigations in annular flows concern purely viscous fluids obeying the power law model, and yield stress fluids obeying the Bingham plastic or the Herschel–Bulkley models. For viscoelastic fluids, investigations are scarcer. Among the first to study viscoelastic annular flows was Bhatnagar [2], who used a Rivlin–Eriksen model to investigate low Reynolds number flow ($Re = 1$) in a concentric geometry, with no cylinder rotation, but in the presence of suction and injection at the cylinder walls. With rotation of the inner cylinder, Dierckes and Schowalter [3] measured the laminar annular flow of polyisobutelene solutions and confirmed that the symmetric flow could be predicted from an inelastic theory based on a power law fitted to the experimental rheological data. Kaloni [4] and Kulshrestha [5] derived analytical solutions for viscoelastic fluids obeying Oldroyd's equations. Pinho and Oliveira [6] solved analytically the concentric annular laminar flow without inner cylinder rotation for the simplified PTT model. They provided expressions for the velocity and stress profiles as well as for the friction factor as a function of the Reynolds and Deborah numbers and the radius ratio. That work is the immediate predecessor of the present investigation since the adopted rheological constitutive equation is the same.

* Corresponding author.
E-mail addresses: doac@ufpa.br (D.O.A. Cruz), fpinho@dem.uminho.pt (F.T. Pinho).

0377-0257/$ – see front matter © 2004 Elsevier B.V. All rights reserved.
doi:10.1016/j.jnnfm.2004.03.007

Nomenclature

$\tilde{c}_2$	normalised constant of integration: $2c_2/(p_{,z}\delta^2)$ (annulus), $c_2/(p_{,z}\delta)$ (channel)
$\tilde{c}_3$	normalised constant of integration, c_3/U
$\tilde{c}_4$	normalised constant of integration: $c_4\delta/U$ (annulus), c_4/U (channel)
C_F	force coefficient in the channel, $-F\delta/(\eta U_P)$
C_M	torque coefficient in the annulus, $-M(R_O^2 - R_I^2)/(4\pi\omega\eta R_O^2 R_I^2)$
De	Deborah number based on axial bulk velocity U, $\lambda U/\delta$
De_c	Deborah number based on U_c, $\lambda U_c/\delta$
De_p	Deborah number based on U_P, $\lambda U_P/\delta$ (channel)
De_T	Deborah number based on U_T, $\lambda U_T/\delta$
De_{T_i}	Deborah number based on tangential velocity of inner cylinder, $\lambda\omega R_I/\delta$ (annulus)
D_H	hydraulic diameter in annulus and channel, 2δ (m)
f	Fanning friction factor, $-\delta(\mathrm{d}p/\mathrm{d}z)/(\rho U^2)$
$f(tr\tau) = f(\tau_{ii})$	stress function of PTT model
F	force per unit area in channel flow (N/m^2)
M	torque per unit length of cylinder (Nm/m)
p	pressure (Pa)
$p_{,z}$	axial pressure gradient, $\partial p/\partial z$ (Pa/m)
r	radial/transverse coordinate (m)
Re	Reynolds number, $Re = \rho U 2\delta/\eta$
R_I	inner cylinder radius (m)
R_O	outer cylinder radius (m)
T	rotational/transverse Reynolds number: $T = \rho\omega R_I\delta/\eta$ (annulus), $T = \rho U_P\delta/\eta$ (channel)
Ta	Taylor number, $Ta = \rho^2\omega^2 R_I\delta^3/\eta^2$
T_{ij}	normalised stress, $\tau_{ij}/(\eta(U_{ch}/\delta))$ with $U_{ch} = U_c$ or U_T
u	axial/longitudinal component of velocity (m/s)
U	axial/longitudinal bulk velocity (m/s)
U_c	characteristic axial/longitudinal velocity scale: $-p_{,z}\delta^2/8\eta$ (annulus), $-p_{,z}\delta^2/3\eta$ (channel) (m/s)
U_{ch}	characteristic velocity (in general) (m/s)
U_P	velocity of lower plate (channel)
U_T	characteristic tangential/spanwise velocity scale: $M/(\pi\eta\delta)$ (annulus), $F\delta/\eta$ (channel) (m/s)
v	tangential/spanwise component of velocity (m/s)
y	normalised radial/ transverse coordinate, r/δ
z	axial/longitudinal coordinate (m)

Greek letters

δ	gap in annulus or in channel, $R_O - R_I$ (m)
ε	parameter in PTT model
η	viscosity parameter in PTT model (Pa s)
κ	radius ratio, R_I/R_O
λ	relaxation time in PTT model (s)
θ	tangential angular coordinate (annulus), spanwise (linear) coordinate (channel)
τ_{ij}	stress component ij (Pa)
ω	angular velocity of inner cylinder in annulus (rad/s)
ξ	velocity ratio, $\omega R_I/U$

Other analytical studies of swirling viscoelastic flows in the literature have been motivated by applications in rheology and tribology. The journal bearing flow has been the source of much work: Beris et al. [7] studied the tangential flow of Maxwell, White-Metzner and CEF fluids in concentric and eccentric annuli using a perturbation theory, and for other fluids the reader is referred to Bird et al. [8]. Rheometrical flows were investigated much earlier, with Coleman et al. [9] providing an extensive review of their characteristics. Studies of secondary effects in these rheometrical flows was of concern especially in the sixties and seventies as in Giesekus [10] or Walters and Waters [11] who investigated the flow in the cone–plate system. For the flow between circular plates, the onset of instabilities was investigated by Joseph [12] following Hill's [13] experiments.

The rod climbing effect, and its sibling without a rod, have also been a major motivation of research, often numerical like that of Debbaut and Hocq [14]. A major contributor to these studies was Joseph and his co-workers: Joseph [15] summarises his many contributions.

There are a few other investigations specifically on the topic of viscoelastic annular flows with and without inner cylinder rotation, but under turbulent flow conditions as in Nouri et al. [16] and Escudier et al. [17].

The objective of the present paper is to analyse in detail the laminar flow of viscoelastic fluids obeying the Phan–Thien–Tanner model in concentric annuli with inner cylinder rotation. In the limit of very thin annulus this solution is well approximated by the simpler solution for the skewed Poiseuille–Couette flow in a channel for which a full analytical solution is also presented. Here, there is a pressure driven Poiseuille flow in the longitudinal direction combined with Couette flow in the spanwise direction. This flow condition has not been previously investigated: the closer to this is the analytical solution for Poiseuille–Couette flow of PTT fluids in the same direction by Hashemabadi et al. [18], an obviously different flow condition given the non-linearities of the fluid constitutive equation.

The paper is organised as follows: in the next section the relevant equations are presented and the various non-dimensional numbers are defined. In Section 3, the an-

alytical solutions are derived for the cylindrical and planar geometries and in Section 4 the results corresponding to the annular flow are plotted and the effect of rotation investigated. A summary of the main conclusions closes the paper.

2. Governing equations

Two similar flows are under investigation here. First, the helical flow in a concentric annulus of inner and outer radius R_I and R_O, respectively, defining an annular gap, $\delta \equiv R_O - R_I$, and radius ratio, $\kappa \equiv R_I/R_O$. The flow is fully-developed, so both the axial velocity, u, and the tangential velocity, v, are only functions of the radial coordinate r and the imposed axial pressure gradient is constant. The second flow condition is the corresponding planar case, with longitudinal velocity, u, and spanwise velocity v, both functions of the transverse coordinate, r. In both cases the wall at $r = R_I$ moves (inner wall/lower plate): it rotates with angular velocity ω in the annulus and moves in the spanwise direction with linear velocity U_P in the channel. Under these conditions the momentum equations are

$$\frac{1}{r^n}\frac{\mathrm{d}}{\mathrm{d}r}(r^n\tau_{rz}) - \frac{\partial p}{\partial z} = 0, \tag{1}$$

$$-\rho n\frac{v^2}{r} = \frac{1}{r^n}\frac{\mathrm{d}}{\mathrm{d}r}(r^n\tau_{rr}) - n\frac{\tau_{\theta\theta}}{r} - \frac{\partial p}{\partial r}, \tag{2}$$

$$\frac{\mathrm{d}}{\mathrm{d}r}(r^{2n}\tau_{r\theta}) = 0, \tag{3}$$

where z refers to the axial or longitudinal direction in the annulus and channel, respectively, r is the radial or transverse direction and θ is the tangential or spanwise directions. Parameter n takes the value of 1 for the axisymmetric geometry and of 0 in the planar case.

The extra stresses are given here by the simplified form of the PTT constitutive equation [19]

$$f(\mathrm{tr}(\boldsymbol{\tau}))\boldsymbol{\tau} + \lambda\overset{\triangledown}{\boldsymbol{\tau}} = 2\eta\boldsymbol{D} \quad \text{with} \quad f(\mathrm{tr}(\boldsymbol{\tau})) = 1 + \frac{\varepsilon\lambda}{\eta}\mathrm{tr}(\tau), \tag{4}$$

where $\boldsymbol{D}$ is the deformation rate tensor, λ is the relaxation time, η is the viscosity coefficient and ε is a parameter of the model limiting the extensional viscosity of the fluid. The stress function $f(\mathrm{tr}(\boldsymbol{\tau}))$, defined in Eq. (4), is the linearization of the more general exponential coefficient and $\overset{\triangledown}{\boldsymbol{\tau}}$ denotes Oldroyd's upper convective derivative

$$\overset{\triangledown}{\boldsymbol{\tau}} = \frac{D\boldsymbol{\tau}}{Dt} - \boldsymbol{\tau}\cdot\nabla\boldsymbol{u} - (\nabla\boldsymbol{u})^{\mathrm{T}}\cdot\boldsymbol{\tau}. \tag{5}$$

For this flow geometry the constitutive equation simplifies to

$$\tau_{rr} = 0, \tag{6}$$

$$\tau_{zz} = \frac{2\lambda\eta}{f(\tau_{ii})^2}\left(\frac{\mathrm{d}u}{\mathrm{d}r}\right)^2, \tag{7}$$

$$\tau_{\theta\theta} = \frac{2\lambda\eta}{f(\tau_{ii})^2}\left[r^n\frac{\mathrm{d}}{\mathrm{d}r}\left(\frac{v}{r^n}\right)\right]^2, \tag{8}$$

$$\tau_{r\theta} = \frac{\eta r^n}{f(\tau_{ii})}\frac{\mathrm{d}}{\mathrm{d}r}\left(\frac{v}{r^n}\right), \tag{9}$$

$$\tau_{rz} = \frac{\eta}{f(\tau_{ii})}\frac{\mathrm{d}u}{\mathrm{d}r}, \tag{10}$$

$$\tau_{\theta z} = \frac{2\lambda\eta r^n}{f(\tau_{ii})^2}\frac{\mathrm{d}u}{\mathrm{d}r}\frac{\mathrm{d}}{\mathrm{d}r}\left(\frac{v}{r^n}\right), \tag{11}$$

where the stress coefficient $f(\tau_{ii})$ was used for compactness. The stress coefficient is now given by the non-linear cubic equation (Eq. (12))

$$f(\tau_{ii}) = 1 + \frac{2\varepsilon\lambda^2}{f(\tau_{ii})^2}\left[\left(\frac{\mathrm{d}u}{\mathrm{d}r}\right)^2 + \left(r^n\frac{\mathrm{d}}{\mathrm{d}r}\left(\frac{v}{r^n}\right)\right)^2\right]. \tag{12}$$

The boundary conditions for this problem express no-slip at the walls and are given by:

$$r = R_I \Rightarrow u = 0,\ v = \omega R_I (\text{or } v = U_P \text{ for the channel}),$$

$$r = R_O \Rightarrow u = 0,\ v = 0.$$

3. Analytical solution

Although initially there are many similarities between the axisymmetric and planar solutions, for the sake of clarity the two cases are presented separately, starting with the helical flow.

3.1. Flow in the annular geometry

Introducing the torque per unit length of the cylinder (M), integration of Eq. (3) gives the variation of the stress component $\tau_{r\theta}$

$$\tau_{r\theta} = \frac{M}{2\pi r^2}. \tag{13}$$

Substituting this result into Eq. (9) provides the following expression

$$r\frac{\mathrm{d}}{\mathrm{d}r}\left(\frac{v}{r}\right) = \frac{M}{2\pi\eta r^2}f(\tau_{ii}), \tag{14}$$

that can be used to calculate $\tau_{\theta\theta}$ in Eq. (8). The tangential normal stress $\tau_{\theta\theta}$ is thus given by

$$\tau_{\theta\theta} = \frac{\lambda M^2}{2\pi^2\eta r^4}. \tag{15}$$

Now, using this result into the radial momentum equation (Eq. (2) gives

$$r\frac{\partial p}{\partial r} = \rho v^2 - \frac{\lambda M^2}{2\pi^2\eta r^4}, \tag{16}$$

which provides the radial distribution of pressure once the radial variation of the tangential velocity is known.

To obtain the axial velocity it is still necessary to deduce expressions for τ_{rz} and τ_{zz}, that depend only on derivatives of velocity and pressure. Eq. (1) can be integrated into

$$\tau_{rz} = \frac{\partial p}{\partial z}\frac{r}{2} + \frac{c_2}{r}, \tag{17}$$

where c_2 is an integration constant. With τ_{rz} also given by Eq. (10), the stress coefficient function is determined as

$$f(\tau_{ii}) = \frac{\eta(\mathrm{d}u/\mathrm{d}r)}{(\partial p/\partial z)(r/2) + (c_2/r)}. \tag{18}$$

Squaring this function and using it in Eq. (7) leads to

$$\tau_{zz} = \frac{2\lambda}{\eta}\left[\frac{\partial p}{\partial z}\frac{r}{2} + \frac{c_2}{r}\right]^2. \tag{19}$$

Now, it is possible to determine the axial and tangential velocity profiles.

According to Eq. (18) and the definition of $f(\tau_{ii})$

$$\eta\frac{\mathrm{d}u}{\mathrm{d}r} = \left[1 + \frac{\lambda\varepsilon}{\eta}(\tau_{\theta\theta} + \tau_{zz})\right]\left[\frac{\partial p}{\partial z}\frac{r}{2} + \frac{c_2}{r}\right], \tag{20}$$

so that, after substitution of Eqs. (15) and (19), the following expression for the axial velocity gradient is deduced

$$\frac{\mathrm{d}u}{\mathrm{d}r} = \frac{1}{\eta}\left[\frac{\partial p}{\partial z}\frac{r}{2} + \frac{c_2}{r}\right] + \frac{2\lambda^2\varepsilon}{\eta^3}\left[\frac{\partial p}{\partial z}\frac{r}{2} + \frac{c_2}{r}\right]\left\{\frac{M^2}{4\pi^2 r^4} + \left[\frac{\partial p}{\partial z}\frac{r}{2} + \frac{c_2}{r}\right]^2\right\}. \tag{21}$$

Using Eqs. (14) and (18), the shear stress $\tau_{\theta z}$ can also be simplified to

$$\tau_{\theta z} = \frac{\lambda M}{\pi\eta r^2}\left[\frac{\partial p}{\partial z}\frac{r}{2} + \frac{c_2}{r}\right]. \tag{22}$$

A solution in terms of non-dimensional quantities is sought. Therefore, for simplicity and prior to integration, the following characteristic parameters are defined: a characteristic axial velocity scale $U_\mathrm{c} = (-p_{,z}\delta^2/8\eta)$, a characteristic tangential velocity scale $U_\mathrm{T} = (M/\pi\eta\delta)$, and the corresponding characteristic Deborah numbers $De_\mathrm{c} = (\lambda U_\mathrm{c}/\delta)$ and $De_\mathrm{T} = (\lambda U_\mathrm{T}/\delta)$. Alternative Deborah numbers are defined on the basis of the axial bulk velocity (U leading to $De \equiv \lambda U/\delta$) and of the tangential velocity of the inner surface of the annulus ($U_{\mathrm{T_i}} = \omega R_\mathrm{I}$ leading to $De_{\mathrm{T_i}} = \lambda U_{\mathrm{T_i}}/\delta$).

This problem requires five independent non-dimensional quantities to characterise the flow: ε and a Deborah number related to the axial flow (De or De_c) are constitutive parameters, the radius ratio κ is a geometric parameter, and finally the Deborah number related to the rotating flow (De_T or $De_{\mathrm{T_i}}$), or alternatively a Taylor number or a rotational Reynolds number, and the Reynolds number of the axial flow (Re), all of which are dynamical parameters. The Reynolds number of the axial flow is defined as $Re = 2\delta\rho U/\eta$, i.e., it is based on the hydraulic diameter $D_\mathrm{H} = 4A/P = 2\delta$, where A is the cross section area and P is the corresponding wetted perimeter. Elsewhere, δ was used as the length scale.

After normalisation and integration of Eq. (21), the axial velocity profile u/U is given by

$$\frac{u}{U} = -2\frac{U_\mathrm{c}}{U}y^2 - 4\tilde{c}_2\frac{U_\mathrm{c}}{U}\ln y + \frac{\varepsilon De_\mathrm{T}^2}{y^2}\frac{U_\mathrm{c}}{U} + \frac{\varepsilon De_\mathrm{T}^2}{2}\frac{U_\mathrm{c}}{U}\frac{\tilde{c}_2}{y^4} - 32\varepsilon De_\mathrm{c}^2\frac{U_\mathrm{c}}{U}y^4 - 192\varepsilon De_\mathrm{c}^2\frac{U_\mathrm{c}}{U}\tilde{c}_2 y^2 - 384\varepsilon De_\mathrm{c}^2\frac{U_\mathrm{c}}{U}\tilde{c}_2^2\ln y + 64\varepsilon De_\mathrm{c}^2\frac{U_\mathrm{c}}{U}\frac{\tilde{c}_2^3}{y^2} + \tilde{c}_3, \tag{23}$$

where the radial coordinate is presented in normalised form as $y = r/\delta$.

In Eq. (23), the new constant of integration c_3 and constant c_2 appear in normalized form: $\tilde{c}_2 \equiv 2c_2/p_{,z}\delta^2$ and $\tilde{c}_3 \equiv c_3/U$. From Eq. (14), and using the stresses of Eqs. (15) and (19), the differential equation for the tangential velocity component becomes

$$r\frac{\mathrm{d}}{\mathrm{d}r}\left(\frac{v}{r}\right) = \frac{M}{2\pi\eta r^2}\left\{1 + \frac{2\varepsilon\lambda^2}{\eta^2}\left[\frac{M^2}{4\pi^2 r^4} + \left(\frac{\partial p}{\partial z}\frac{r}{2} + \frac{c_2}{r}\right)^2\right]\right\}. \tag{24}$$

After normalisation, the integration of this equation gives the following tangential velocity profile:

$$\frac{v}{U} = -\frac{1}{4y}\frac{U_\mathrm{T}}{U} - \frac{1}{24y^5}\varepsilon De_\mathrm{T}^2\frac{U_\mathrm{T}}{U} + 16\varepsilon De_\mathrm{c}^2\frac{U_\mathrm{T}}{U}y\ln y - 16\varepsilon De_\mathrm{c}^2\frac{U_\mathrm{T}}{U}\frac{\tilde{c}_2}{y} - 4\varepsilon De_\mathrm{c}^2\frac{U_\mathrm{T}}{U}\frac{\tilde{c}_2^2}{y^3} + \tilde{c}_4 y. \tag{25}$$

Eq. (25) introduces a new nondimensional constant of integration, $\tilde{c}_4 = c_4\delta/U$.

Application of the boundary conditions to the velocity profiles provides equations to determine the constants of integration. No-slip condition of the axial velocity at both walls (Eq. (23)) gives the following cubic equation on $\tilde{c}_2$

$$b_0 + b_1\tilde{c}_2 + b_2\tilde{c}_2^2 + b_3\tilde{c}_2^3 = 0, \tag{26}$$

with coefficients

$$b_0 = 2(y_\mathrm{o}^2 - y_\mathrm{i}^2) + \varepsilon De_\mathrm{T}^2\left(\frac{1}{y_\mathrm{i}^2} - \frac{1}{y_\mathrm{o}^2}\right) + 32\varepsilon De_\mathrm{c}^2(y_\mathrm{o}^4 - y_\mathrm{i}^4),$$

$$b_1 = 4\ln\frac{y_\mathrm{o}}{y_\mathrm{i}} - \frac{\varepsilon De_\mathrm{T}^2}{2}\left(\frac{1}{y_\mathrm{o}^4} - \frac{1}{y_\mathrm{i}^4}\right) + 192\varepsilon De_\mathrm{c}^2(y_\mathrm{o}^2 - y_\mathrm{i}^2),$$

$$b_2 = 384\varepsilon De_\mathrm{c}^2\ln\frac{y_\mathrm{o}}{y_\mathrm{i}}, \quad b_3 = -64\varepsilon De_\mathrm{c}^2\left(\frac{1}{y_\mathrm{o}^2} - \frac{1}{y_\mathrm{i}^2}\right), \tag{27}$$

This cubic equation has the following solution

$$\tilde{c}_2 = \mathrm{sign}(p)|p|^{1/3} + \mathrm{sign}(q)|q|^{1/3} - \tfrac{1}{3}a_1, \tag{28}$$

with

$$p = -\frac{b}{2} + \sqrt{d}, \quad q = -\frac{b}{2} - \sqrt{d}, d = \frac{b^2}{4} + \frac{a^3}{27},$$
$$a = a_2 - \frac{a_1^2}{3}, \quad b = a_3 - \frac{a_1 a_2}{3} + \frac{2a_1^3}{27},$$
$$\text{and} \quad a_1 = \frac{b_2}{b_3}, \; a_2 = \frac{b_1}{b_3} \quad \text{and} \quad a_3 = \frac{b_0}{b_3}. \tag{29}$$

Once $\tilde{c}_2$ is known, determination of the other two constants is straightforward: $\tilde{c}_3$ is obtained from Eq. (23) by setting the no-slip condition at any of the walls and $\tilde{c}_4$ is calculated with Eq. (25) applying the no-slip condition at the outer wall. The axial cross section average velocity can be calculated from its definition for the annulus

$$U = \frac{2(1-\kappa)}{1+\kappa} \int_{y_\mathrm{i}}^{y_\mathrm{o}} uy \, \mathrm{d}y. \tag{30}$$

Substituting the velocity variation of Eq. (23) and performing the integration, the following expression is obtained

$$U = \frac{2(1-\kappa)}{1+\kappa} \left[-\frac{1}{2} U_\mathrm{c} (y_\mathrm{o}^4 - y_\mathrm{i}^4) - 2\tilde{c}_2 U_\mathrm{c} \left(\frac{y_\mathrm{i}^2}{2} - \frac{y_\mathrm{o}^2}{2} + y_\mathrm{o}^2 \ln y_\mathrm{o} - y_\mathrm{i}^2 \ln y_\mathrm{i} \right) \right.$$
$$+ \varepsilon De_\mathrm{T}^2 U_\mathrm{c} \ln \frac{y_\mathrm{o}}{y_\mathrm{i}} - \frac{\varepsilon De_\mathrm{T}^2}{4} U_\mathrm{c} \tilde{c}_2 \left(\frac{1}{y_\mathrm{o}^2} - \frac{1}{y_\mathrm{i}^2} \right) - \frac{16}{3} \varepsilon De_\mathrm{c}^2 U_\mathrm{c} (y_\mathrm{o}^6 - y_\mathrm{i}^6) - 48 \varepsilon De_\mathrm{c}^2 U_\mathrm{c} \tilde{c}_2 (y_\mathrm{o}^4 - y_\mathrm{i}^4)$$
$$\left. + \; 192 \varepsilon De_\mathrm{c}^2 U_\mathrm{c} \tilde{c}_2^2 \left(\frac{y_\mathrm{i}^2}{2} - \frac{y_\mathrm{o}^2}{2} + y_\mathrm{o}^2 \ln y_\mathrm{o} - y_\mathrm{i}^2 \ln y_\mathrm{i} \right) + 64 \varepsilon De_\mathrm{c}^2 U_\mathrm{c} \tilde{c}_2^3 \ln \frac{1}{\kappa} + \frac{\tilde{c}_3}{2} (y_\mathrm{o}^2 - y_\mathrm{i}^2) \right] \tag{31}$$

Setting $v = \omega y_\mathrm{i} \delta$ at $y = y_\mathrm{i}$ in Eq. (25) gives the angular rotational speed

$$\omega = \frac{1}{y_\mathrm{i} \delta} \left[-\frac{U_\mathrm{T}}{4 y_\mathrm{i}} - \frac{\varepsilon De_\mathrm{T}^2}{24} \frac{U_\mathrm{T}}{y_\mathrm{i}^5} + 16 U_\mathrm{T} \varepsilon De_\mathrm{c}^2 y_\mathrm{i} \ln y_\mathrm{i} \right.$$
$$\left. - 16 U_\mathrm{T} \varepsilon De_\mathrm{c}^2 y_i \ln y_\mathrm{i} \frac{\tilde{c}_2}{y_\mathrm{i}} - 4 U_\mathrm{T} \varepsilon De_\mathrm{c}^2 \frac{\tilde{c}_2^2}{y_\mathrm{i}^3} + \delta \tilde{c}_4 y_\mathrm{i} \right]. \tag{32}$$

The stress field can also be presented in nondimensional form using the various non-dimensional parameters discussed above. Next, note the different velocity scales used to normalise axial related and rotation related stress tensor components. The exception is $\tau_{\theta z}$ which can be normalised in both ways, as indicated below.

$$T_{rz} \equiv \frac{\tau_{rz}}{\eta (U_\mathrm{c}/\delta)} = -4 \left(y + \frac{\tilde{c}_2}{y} \right), \tag{33}$$

$$T_{r\theta} \equiv \frac{\tau_{r\theta}}{\eta (U_\mathrm{T}/\delta)} = \frac{1}{2y^2}, \tag{34}$$

$$T_{zz} \equiv \frac{\tau_{zz}}{\eta (U_\mathrm{c}/\delta)} = 2 De_\mathrm{c} T_{rz}^2 = 32 De_\mathrm{c} \left(y + \frac{\tilde{c}_2}{y} \right)^2, \tag{35}$$

$$T_{\theta\theta} \equiv \frac{\tau_{\theta\theta}}{\eta (U_\mathrm{T}/\delta)} = 2 De_\mathrm{T} T_{r\theta}^2 = \frac{De_\mathrm{T}}{2y^4}, \tag{36}$$

$$T_{\theta z} \equiv \frac{\tau_{\theta z}}{\eta (U_\mathrm{T}/\delta)} = 2 De_\mathrm{c} T_{r\theta} T_{rz} = -\frac{4 De_\mathrm{c}}{y^2} \left[y + \frac{\tilde{c}_2}{y} \right] \quad \text{or}$$
$$T'_{\theta z} \equiv \frac{\tau_{\theta z}}{\eta (U_\mathrm{c}/\delta)} = 2 De_\mathrm{T} T_{r\theta} T_{rz} = -\frac{4 De_\mathrm{T}}{y^2} \left[y + \frac{\tilde{c}_2}{y} \right]. \tag{37}$$

The axial pressure gradient is more conveniently written as the Fanning friction factor f and, as shown in Pinho and Oliveira [6], in the case of the PTT model it is given by

$$fRe = 16 \frac{U_\mathrm{c}}{U}, \tag{38}$$

which can be compared with the corresponding expression for Newtonian fluids

$$(fRe)_\mathrm{N} = 16 \frac{1}{(1+\kappa)^2/(1-\kappa)^2 - (1+\kappa)/(1-\kappa)(1/\ln(1/\kappa))}. \tag{39}$$

The torque required to rotate the inner cylinder is usually quantified by a torque coefficient C_M defined in such way that it is unity for Newtonian fluids (note that M is torque per unit length).

$$C_M \equiv -\frac{M(R_\mathrm{o}^2 - R_\mathrm{i}^2)}{4\pi\omega\eta R_\mathrm{o}^2 R_\mathrm{i}^2}, \tag{40}$$

For this flow, it can be shown that C_M is given by

$$C_M = -\frac{U_\mathrm{T}}{U_{\mathrm{T_i}}} \frac{(1-\kappa^2)(1-\kappa)}{4\kappa}, \tag{41}$$

Finally, to quantify the rotation it is usual to use either the rotational Reynolds number

$$T = \frac{\rho\omega R_\mathrm{I} \delta}{\eta}, \tag{42}$$

or alternatively the Taylor number

$$Ta = \left(\frac{\rho\omega}{\eta} \right)^2 R_\mathrm{I} \delta^3. \tag{43}$$

These numbers are related to each other and to $De_{\mathrm{T_i}}$ as below

$$T = \frac{\mathrm{Re}}{2De} De_{\mathrm{T_i}}, \tag{44}$$

$$Ta = \left(\frac{1}{\kappa} - 1 \right) T^2 = \left(\frac{1}{\kappa} - 1 \right) \left(\frac{Re}{2De} \right)^2 De_{\mathrm{T_i}}^2. \tag{45}$$

The combination of Re, De and $De_{\mathrm{T_i}}$ into those more typical nondimensional numbers, makes them more difficult to use analytically.

3.2. Flow in the planar case

The solution for the planar case follows the same steps as for the annulus, but is simpler and for brevity is presented here with less detail.

Instead of a torque, the lower plate moves by action of a force per unit area, F, and integration of Eq. (3), and subsequent substitutions (see Section 3.1), give

$$\tau_{\theta r} = F, \tag{46}$$

$$\tau_{\theta\theta} = \frac{2\lambda F^2}{\eta}, \tag{47}$$

and a null transverse distribution of pressure ($\partial p/\partial r = 0$), i.e. now the pressure only varies with the longitudinal coordinate in contrast to the annular case where it also depends on r.

The stresses τ_{rz}, τ_{zz} and the stress coefficient function are given by

$$\tau_{rz} = \frac{\mathrm{d}p}{\mathrm{d}z} r + c_2, \tag{48}$$

$$\tau_{zz} = \frac{2\lambda}{\eta}\left[\frac{\mathrm{d}p}{\mathrm{d}z} r + c_2\right]^2, \tag{49}$$

$$f(\tau_{ii}) = \frac{\eta(\mathrm{d}u/\mathrm{d}r)}{(\mathrm{d}p/\mathrm{d}z)r + c_2}. \tag{50}$$

Combining the various equations gives

$$\tau_{\theta z} = \frac{2\lambda F}{\eta}\left[\frac{\mathrm{d}p}{\mathrm{d}z} r + c_2\right], \tag{51}$$

and the equation to be integrated for the longitudinal velocity profile

$$\frac{\mathrm{d}u}{\mathrm{d}r} = \frac{1}{\eta}\left[\frac{\mathrm{d}p}{\mathrm{d}z} r + c_2\right] + \frac{2\lambda^2\varepsilon}{\eta^3}\left[\frac{\mathrm{d}p}{\mathrm{d}z} r + c_2\right]\left\{F^2 + \left[\frac{\mathrm{d}p}{\mathrm{d}z} r + c_2\right]^2\right\}. \tag{52}$$

The following non-dimensional quantities are used in the planar case: the longitudinal characteristic velocity scale $U_{\mathrm{c}} = -p_{,z}\delta^2/(3\eta)$, the characteristic spanwise velocity scale $U_{\mathrm{T}} = F\delta/\eta$ and the corresponding Deborah numbers defined as for the annulus. The alternative Deborah numbers are $De = \lambda U/\delta$ and $De_{\mathrm{p}} = \lambda U_{\mathrm{P}}/\delta$, this latter taking over the role of De_{Ti} for the annulus. The Reynolds number and the hydraulic diameter are also identical to those used in the annular flow case.

The normalised transverse coordinate y is also defined as $y = r/\delta$ and the normalised longitudinal velocity profile is given by

$$\frac{u}{U} = -3\frac{U_{\mathrm{c}}}{U}[y + \tilde{c}_2]^2\left\{\frac{1}{2} + \varepsilon De_{\mathrm{T}}^2 + \frac{9}{2}\varepsilon De_{\mathrm{c}}^2[y + \tilde{c}_2]^2\right\} + \tilde{c}_3, \tag{53a}$$

or alternatively

$$\frac{u}{U} = 3\frac{U_{\mathrm{c}}}{U}(y_i - y)(y - y_{\mathrm{o}}) \times \left\{\frac{1}{2} + \varepsilon De_{\mathrm{T}}^2 + \frac{9}{2}\varepsilon De_{\mathrm{c}}^2\left[\frac{1}{4} + (y + \tilde{c}_2)^2\right]\right\}, \tag{53b}$$

where the normalised constants of integration are $\tilde{c}_2 \equiv c_2/(p_{,z}\delta)$ and $\tilde{c}_3 \equiv c_3/U$.

The spanwise velocity profile in non-dimensional form is

$$\frac{v}{U} = \frac{U_{\mathrm{T}}}{U} y[1 + 2\varepsilon De_{\mathrm{T}}^2 + 6\varepsilon De_{\mathrm{c}}^2 y^2 + 18\varepsilon De_{\mathrm{c}}^2 y\tilde{c}_2 + 18\varepsilon De_{\mathrm{c}}^2\tilde{c}_2^2] + \tilde{c}_4, \tag{54}$$

with $\tilde{c}_4 \equiv c_4/U$.

As in the annular case, application of the boundary conditions determine the constants of integration, but here, in contrast, an explicit equation gives $\tilde{c}_2$ as

$$\tilde{c}_2 = -\tfrac{1}{2}(y_{\mathrm{o}} + y_{\mathrm{i}}), \tag{55}$$

and

$$\tilde{c}_3 = \frac{3}{4}\frac{U_{\mathrm{c}}}{U}\left[\frac{1}{2} + \varepsilon De_{\mathrm{T}}^2 + \frac{9}{8}\varepsilon De_{\mathrm{c}}^2\right]. \tag{56}$$

The longitudinal bulk velocity is obtained from its definition for the planar case

$$U = \int_{y_{\mathrm{i}}}^{y_{\mathrm{o}}} u\,\mathrm{d}y = U_{\mathrm{c}}\left[\frac{1}{4} + \frac{\varepsilon De_{\mathrm{T}}^2}{2} + \frac{27}{40}\varepsilon De_{\mathrm{c}}^2\right]. \tag{57}$$

The velocity of the lower plate is related to U_{T} via

$$U_{\mathrm{P}} = -U_{\mathrm{T}}(1 + 2\varepsilon De_{\mathrm{T}}^2 + \tfrac{3}{2}\varepsilon De_{\mathrm{c}}^2). \tag{58}$$

The stress field in non-dimensional form is therefore given by

$$T_{rz} \equiv \frac{\tau_{rz}}{\eta(U_{\mathrm{c}}/\delta)} = -3(y + \tilde{c}_2), \tag{59}$$

$$T_{r\theta} \equiv \frac{\tau_{r\theta}}{\eta(U_{\mathrm{T}}/\delta)} = 1, \tag{60}$$

$$T_{zz} \equiv \frac{\tau_{zz}}{\eta(U_{\mathrm{c}}/\delta)} = 2De_{\mathrm{c}}T_{rz}^2 = 18De_{\mathrm{c}}(y + \tilde{c}_2)^2, \tag{61}$$

$$T_{\theta\theta} \equiv \frac{\tau_{\theta\theta}}{\eta(U_{\mathrm{T}}/\delta)} = 2De_{\mathrm{T}}T_{r\theta}^2 = 2De_{\mathrm{T}}, \tag{62}$$

$$T_{\theta z} \equiv \frac{\tau_{\theta z}}{\eta(U_{\mathrm{T}}/\delta)} = 2De_{\mathrm{c}}T_{r\theta}T_{rz} = -6De_{\mathrm{c}}(y + \tilde{c}_2) \quad \text{or}$$

$$T_{\theta z} \equiv \frac{\tau_{\theta z}}{\eta(U_{\mathrm{c}}/\delta)} = 2De_{\mathrm{T}}T_{r\theta}T_{rz} = -6De_{\mathrm{T}}(y + \tilde{c}_2). \tag{63}$$

The Fanning friction factor is quantified as

$$fRe = 6\frac{U_{\mathrm{c}}}{U}, \tag{64}$$

and the force coefficient

$$C_F = \frac{-F\delta}{\eta U_P} = -\frac{U_T}{U_P}. \quad (65)$$

To quantify the movement of the lower plate, we can use an adequate Reynolds umber, here also referred to as T

$$T \equiv \frac{\rho U_P \delta}{\eta} = \frac{Re}{2De} De_P. \quad (66)$$

A Taylor number can also be defined in analogy to the annular case as

$$Ta \equiv \left(\frac{\rho U_P \delta}{\eta}\right)^2 \frac{\delta}{R_I} = \frac{T^2}{y_i}. \quad (67)$$

The motivation for the derivation of this solution was its use for the limiting condition of flow in very thin annulus ($\kappa \to 1$), hence the specific form of the equations. The above expressions for skewed planar Poiseuille–Couette flow can be further simplified if the lower plate is fixed at the origin of the coordinate system ($y_i = 0$, $y_0 = 1$).

4. Results and discussion

The presentation of results is divided in three parts and concerns only the more difficult helical flow. First, radial profiles of velocity and stress components are shown to illustrate the influence of the various relevant non-dimensional numbers. In the second part, results of more engineering interest are presented for the direct and indirect problems. Finally, it is shown that the simpler equations for the planar case are valid for very thin annuli.

4.1. Detailed flow characteristics

In the absence of inner cylinder rotation ($T_a = 0$), Pinho and Oliveira [6] developed an analytical solution and our solution exactly matches theirs, as it should. Under these conditions, the axial velocity profile and *fRe* are independent of the Reynolds number. The flow behaves essentially as Newtonian for $\varepsilon De^2 < 0.001$, whereas for $\varepsilon De^2 > 10$ the velocity profile is near the high Deborah number asymptotic shape corresponding to a PTT fluid where the shear-thinning viscosity behaviour is present over a very wide range of shear rates (for the viscosity function see [20] or [21], although Keunings and Crochet [22] plotted it much earlier). These profiles are presented in Pinho and Oliveira [6] and consequently are omitted here for conciseness.

As with inelastic power law fluids [1], the rotation of the inner cylinder affects the stress field and this has an impact on the axial velocity. Escudier et al. [1] identified three different flow regimes according to the relative strengths of the axial and tangential flow. If the velocity ratio ξ is less than 1 the flow is dominated by the axial flow, a rotation dominated flow requires a velocity ratio (ξ) larger than 10 and a mixed flow is present in the range $1 < \xi < 10$.

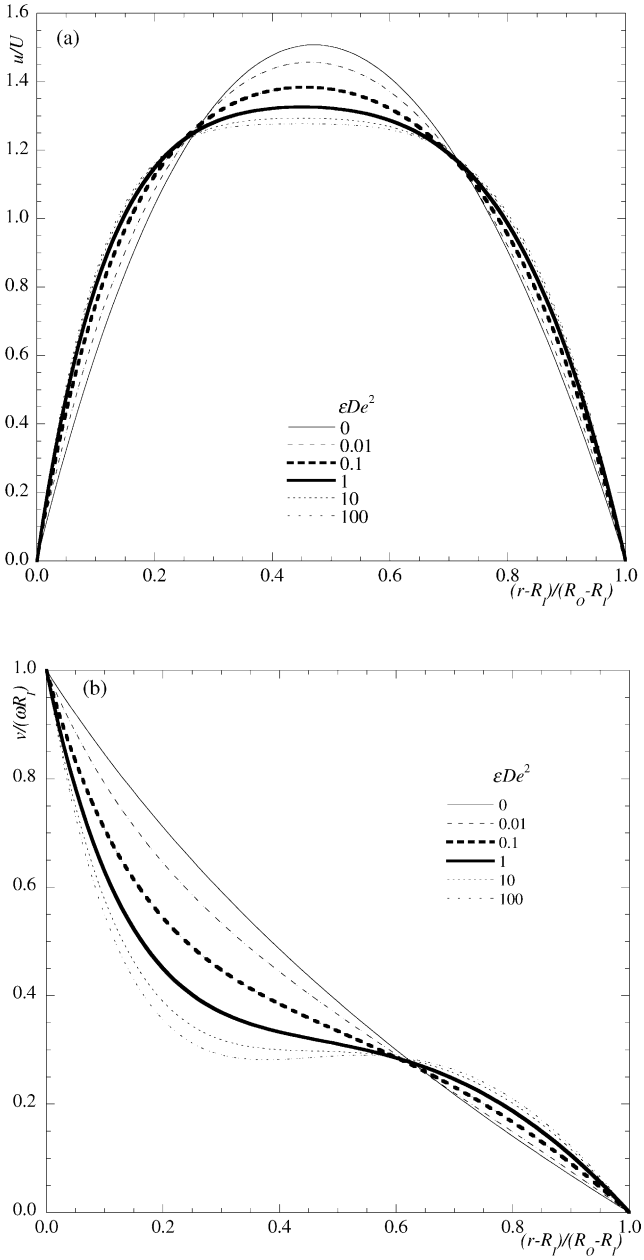

Fig. 1. Radial profiles of the normalised axial (a) and tangential (b) velocities in an annulus of $\kappa = 0.5$ for an SPTT fluid for axial-dominated flow conditions ($Re = 1000$; $Ta = 1000$).

The axial and tangential velocity profiles presented in Figs. 1–3 pertain to each of the above mentioned flow regimes. In the axially-dominated flow regime, the variation of the axial velocity profile in Fig. 1(a) is like that for no cylinder rotation in Pinho and Oliveira [6], with flow elasticity (εDe^2) imparting a plug-like shape. In terms of tangential velocity, the flow elasticity parameter also has a dramatic influence as can be seen in Fig. 1(b). As εDe^2 increases the $v/(\omega R_I)$ profile becomes increasingly distorted to a sigmoidal shape and for εDe^2 in excess of about 10 the profile is no longer monotonic. This behaviour is akin

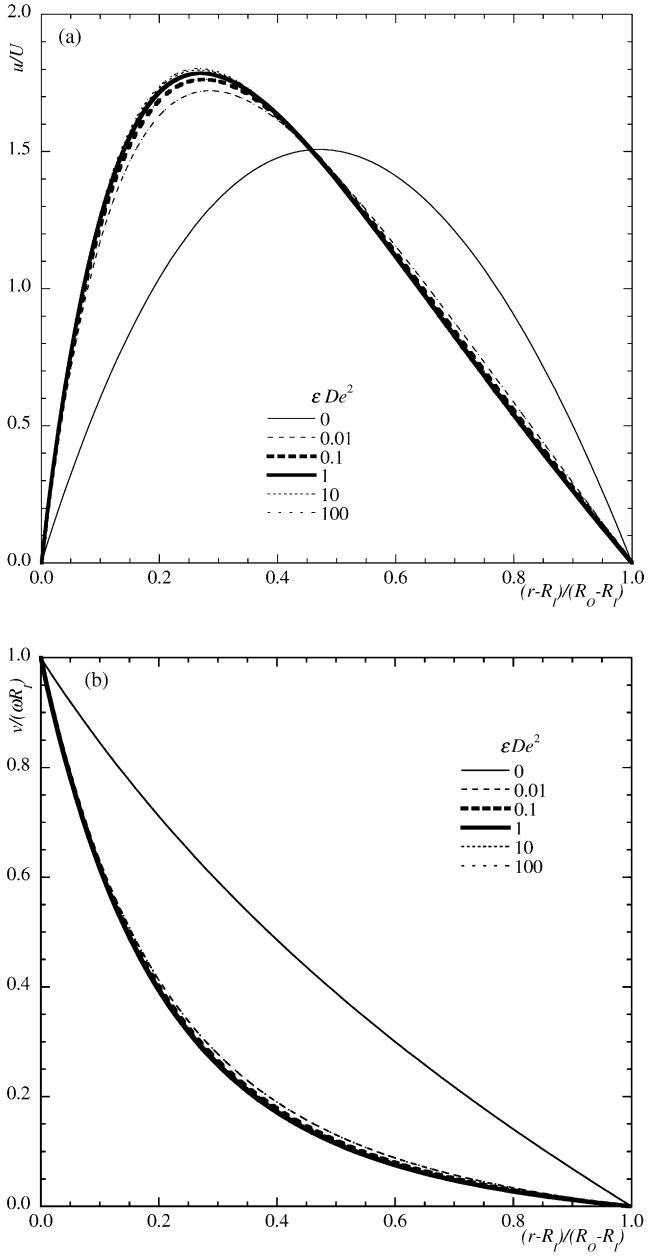

Fig. 2. Radial profiles of the normalised axial (a) and tangential (b) velocities in an annulus of $\kappa = 0.5$ for an SPTT fluid for rotation-dominated flow conditions ($Re = 1$; $Ta = 10{,}000$).

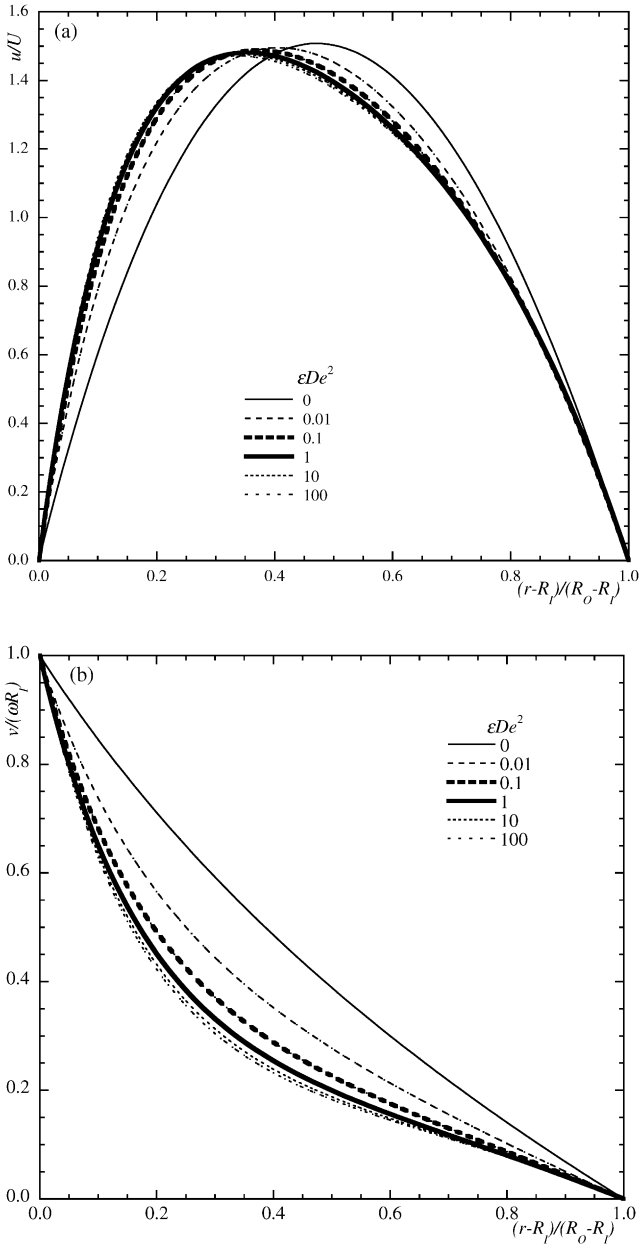

Fig. 3. Radial profiles of the normalised axial (a) and tangential (b) velocities in an annulus of $\kappa = 0.5$ for an SPTT fluid for mixed flow conditions ($Re = 1$; $Ta = 10$).

to that seen by Nouar et al. [23], and also calculated by Escudier et al. [24], and is due to the intense shear-thinning of the viscometric viscosity of the fluids. This sigmoidal shape is easy to understand: for axial-dominated flows and strongly shear-thinning fluids, the viscosity is very low near the walls and high in the centre of the annulus where the shear rate is minimum. Since the stress controlling rotational flow ($\tau_{\theta r}$) varies with radius less than the viscosity, the radial gradient of the tangential velocity must be high close to the walls and small in the center, thus imparting the sigmoidal shape to the v profile. For lower Taylor numbers, leading to ξ below the present value of 0.006325, the same patterns are observed.

For rotation-dominated flow Fig. 2 plots the axial and tangential velocity profiles corresponding to a condition with $\xi = 200$. To understand the observed variations it is important to realise that, whereas in axially dominated flow the shear-thinning behaviour affects the whole annular space, here the high rates of deformation and the shear thinning concentrate near the inner cylinder. Higher values of Ta would increase the extent of such region, but this would correspond to conditions where laminar flow is unstable. In fact, even for Taylor numbers well below 50,000 secondary

flows are known to appear due to flow instabilities in purely azimuthal flow [25]. For the concentric geometry, and in the absence of any elasticity, the PTT model simplifies to the Newtonian behaviour for which there is a perfect decoupling between axial and tangential flows.

As soon as εDe^2 differs from zero both flows are coupled and the axial flow becomes highly distorted towards the inner cylinder and the peak velocities increase around 15% because of the lower viscosities there. Similarly, for the tangential velocity in Fig. 2(b) a strong deviation of the flow towards the inner cylinder is seen. The effect of the Deborah number is also weaker than for $\xi < 1$, because now (for $\xi > 10$) the rates of deformation of the fluid are weaker. Still, a tendency is observed for the maximum axial velocity to decrease and for the profile to widen as εDe^2 increases.

Under the mixed flow conditions in Fig. 3 the axial and tangential velocity profiles show better the progression from the Newtonian decoupled flow to the flow dominated by elasticity as εDe^2 increases. Simultaneously, the progression from the axial dominated flow, where the axial velocity profiles are more central, to the rotation dominated flow where they are distorted toward the inner cylinder, is also evident. This figure corresponds to relatively weak axial and rotational flows hence the rates of deformation are low and εDe^2 is not seen to affect the magnitude of the velocities.

Next, the radial variation of the various stress tensor components is analysed in detail. In Fig. 4(a) the shear stress due to rotation ($\tau_{\theta r}$) is plotted in normalised form; it has a universal form regardless of the values of *Re*, *Ta* and εDe^2. This is immediately clear from inspection of its definition in Eq. (34). In contrast, the definition of the axial shear stress in Eq. (33) shows this component not to be independent of *Re*, *Ta* and εDe^2 via the constant of integration $\tilde{c}_2$ and Fig. 4 also shows its variation. For a Newtonian fluid, or in the absence of rotation, T_{rz} is independent of flow elasticity and balances the axial pressure gradient as is known from Pinho and Oliveira [6]. For an axial-dominated flow there is a weak dependence of T_{rz} on εDe^2, because of the decrease in viscosity due to the rotational flow and this is seen in Fig. 4(a). The dependence on εDe^2 is clearer in Fig. 4(b) which shows the progression of T_{rz} from an independent profile at $\varepsilon De^2 = 0$ towards the profile for a rotation dominated flow. When the flow is dominated by rotation (curves for $Ta = 10{,}000$), the viscosity is basically defined by the rotational flow and the weak dependence of T_{rz} on εDe^2 is due to the slight effect of the axial flow upon the viscosity. Under mixed flow conditions (curves for $Ta = 10$), the viscosity is strongly affected by both the axial and the rotational flow and now the variation of T_{rz} with εDe^2 is stronger, reflecting the changes in viscosity across the annulus. T_{rz} is proportional to the axial velocity gradient hence in axial dominated flows T_{rz} goes to zero near the center of the annulus where the peak velocity occurs. Since rotation deviates the axial flow towards the inner wall, T_{rz} decreases here and increases in the outer wall region as is well shown.

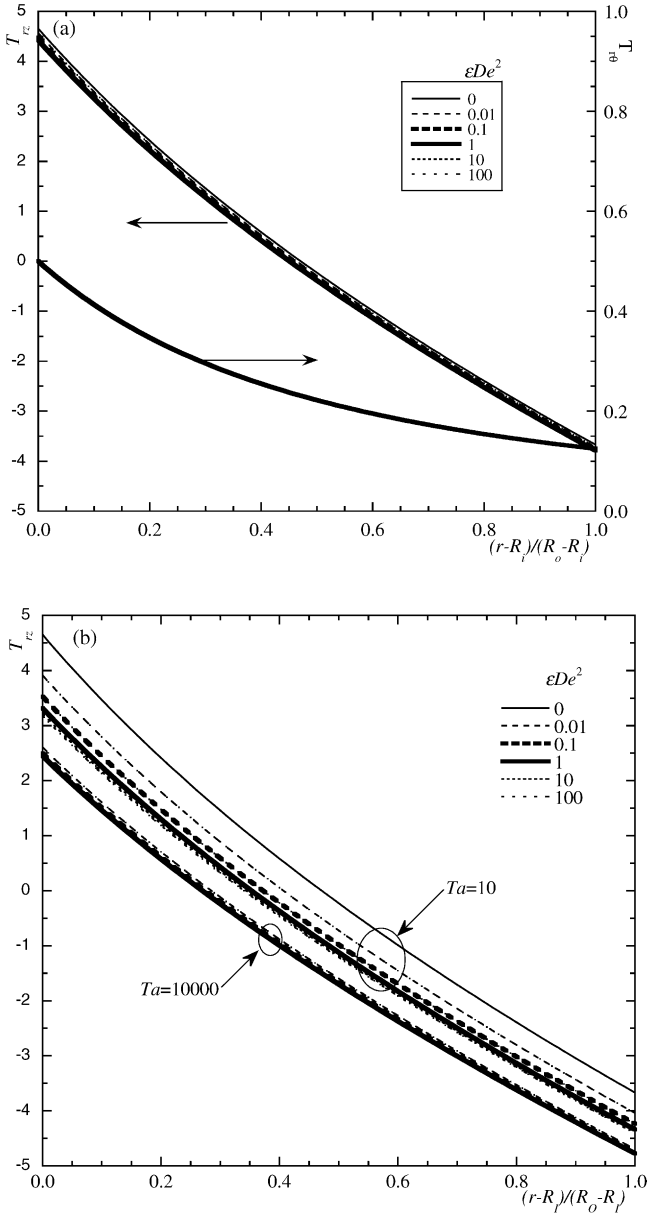

Fig. 4. Radial profiles of the nondimensional shear stresses τ_{rz} and $\tau_{\theta r}$ for an SPTT fluid in annuli with $\kappa = 0.5$: (a) $Re = 1000$, $Ta = 10{,}000$ ($\xi = 0.2$); (b) $Re = 1$ with $Ta = 10$ ($\xi = 6.325$) and $Ta = 10{,}000$ ($\xi = 200$).

Given the combined axial and rotational flow the tangential axial shear stress $\tau_{\theta z}$ is non-zero and is plotted in Fig. 5(a) and (b) for axially-dominated and tangential dominated flow, respectively. The normalised stress plotted uses the tangential characteristic velocity (see definition of $T_{\theta z}$ in Eq. (37)) and is given by the product of $T_{r\theta}$ and T_{rz}. Although the variations of these two stresses with εDe^2 are small, in particular for the two limiting flow conditions, larger variations are observed for $T_{\theta z}$ because the characteristic axial Deborah number De_c varies significantly with εDe^2. As rotation becomes increasingly relevant the value of De_c drops and the variations of $T_{\theta z}$ decrease. Had we

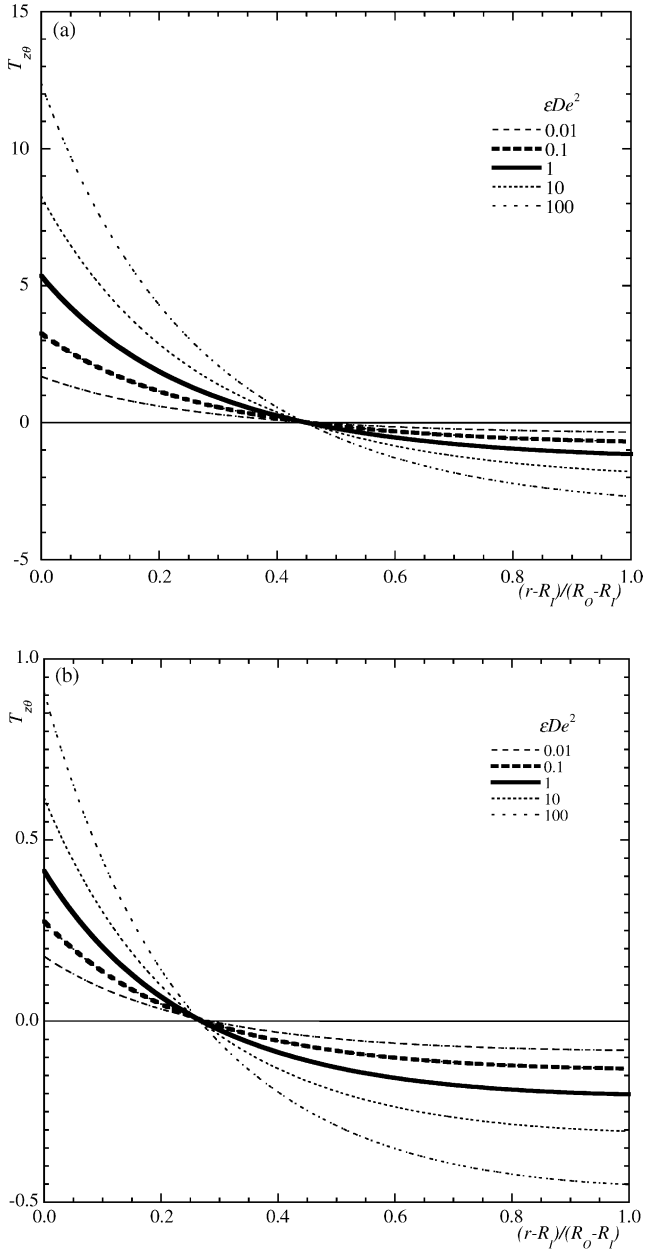

Fig. 5. Radial profiles of the nondimensional $T_{\theta z}$ normal stress of an SPTT fluid in annuli with $\kappa = 0.5$: (a) $Re = 1000$, $Ta = 10{,}000$; (b) $Re = 1$, $Ta = 10{,}000$.

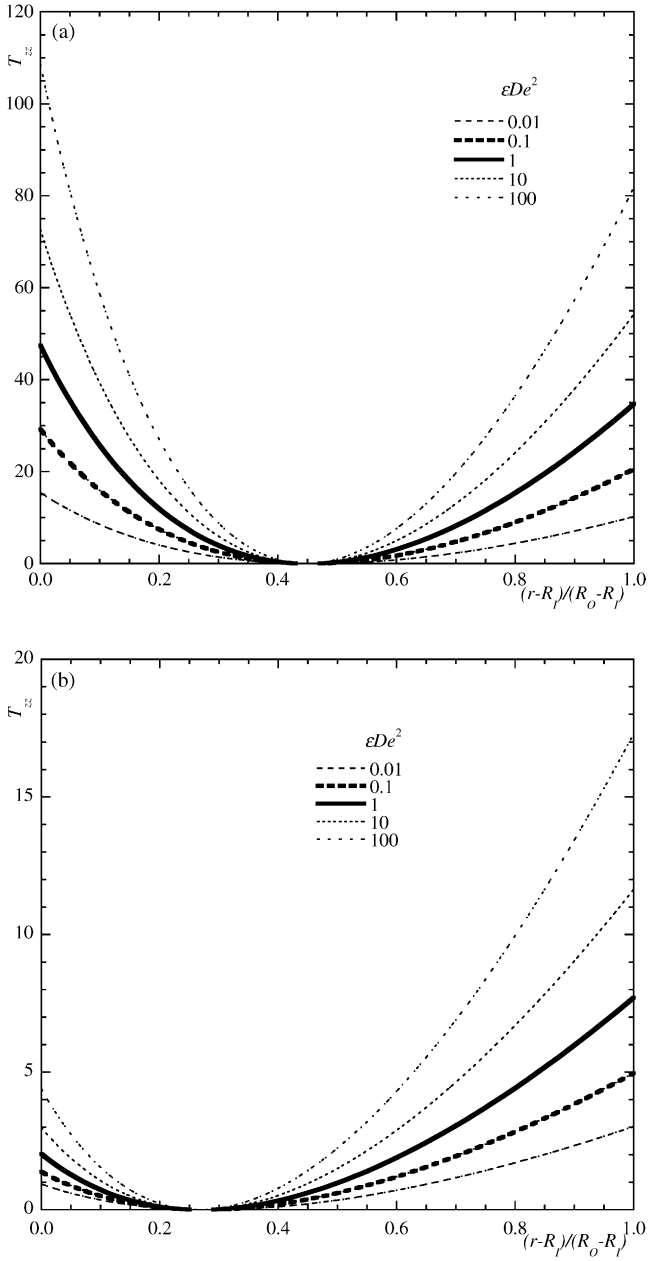

Fig. 6. Radial profiles of the nondimensional T_{zz} normal stress of an SPTT fluid in annuli with $\kappa = 0.5$: (a) $Re = 1000$, $Ta = 10{,}000$; (b) $Re = 1$, $Ta = 10{,}000$.

plotted the alternative tangential-axial stress ($T'_{\theta z}$), similar magnitude of variations would have been observed, but now for axial dominated flow we would see values of $T'_{\theta z}$ 15 times smaller than for tangential dominated flow, because it would be affected by De_{T} rather than by De_{c}.

The axial normal stress variations are shown in Fig. 6. These are exclusively due to the strength of the axial flow, via its radial gradient squared, and fluid elasticity, but are also affected by rotation (cf. Eq. (34) due to the distortions in the axial flow. For axially dominated flows, Fig. 6(a), the stresses increase with flow elasticity and reach maxima of the order of 100 for $\varepsilon De^2 = 100$. As rotation increases in strength, the curves move towards the inner cylinder and the magnitude of the stresses decrease significantly as can be seen in Fig. 6(b); note the different ordinates in Fig. 6(a) and (b) showing a decrease by a factor of 6. As mentioned above, this reduction is due to lower rates of deformation in the rotation dominated flows.

Finally, for the tangential normal stress the behaviour is qualitatively opposite to that of the axial normal stress. $T_{\theta\theta}$ is due to the rotational flow, via the radial gradient of the tangential velocity squared, and fluid elasticity. The effect of the axial flow is more difficult to observe given the monotonic variation of the tangential velocity. Profiles of $T_{\theta\theta}$ are

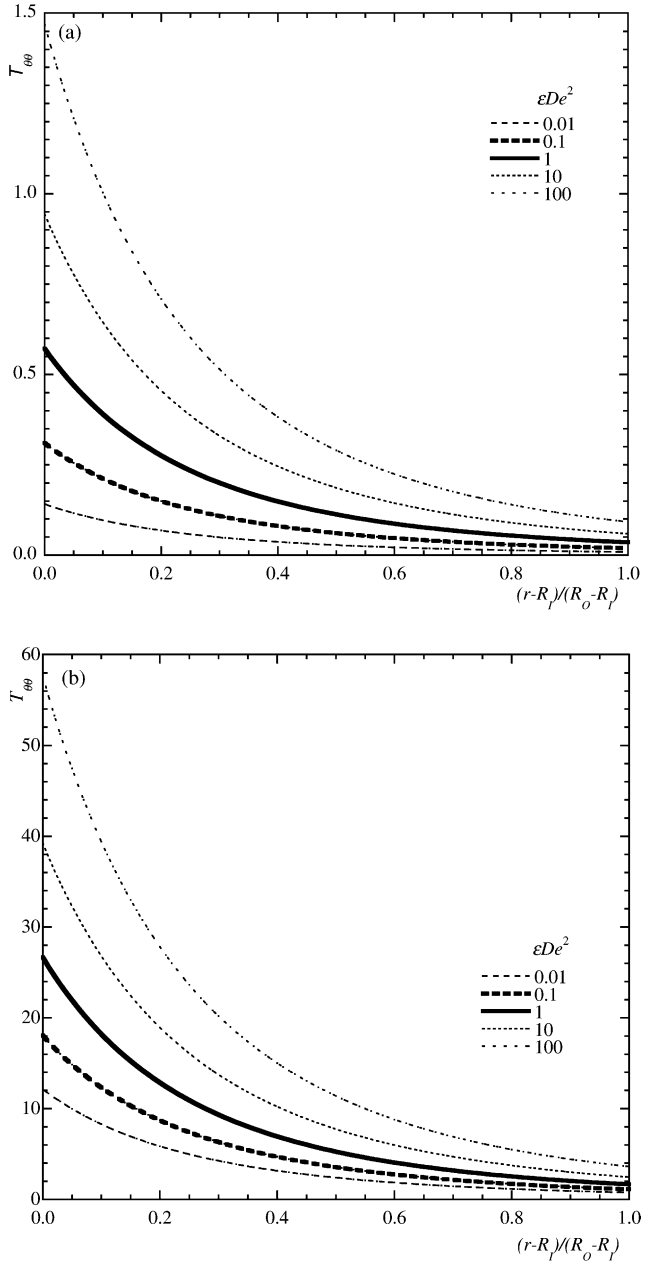

Fig. 7. Radial profiles of the nondimensional $T_{\theta\theta}$ normal stress of an SPTT fluid in annuli with $\kappa = 0.5$: (a) $Re = 1000$, $Ta = 10{,}000$; (b) $Re = 1$, $Ta = 10{,}000$.

plotted in Fig. 7(a) and (b) for axially dominated and rotation dominated flows, respectively. Note the different ordinates in the figures showing values of $T_{\theta\theta}$ in the axially dominated case that are 40 times smaller than in Fig. 7(b).

4.2. Bulk flow characteristics

In analysing the bulk flow characteristics we aim to solve the so-called direct and indirect problems, via universal relations that are based on non-dimensional quantities. All the equations relating the relevant quantities have already been presented in Section 3 and here the focus is on defining the correct sequence of calculations and in plotting the corresponding results as a function of the more useful Reynolds number, the Taylor number and εDe^2.

In the direct problem the Reynolds number (or the axial bulk velocity) and the Taylor number (or rotational speed) are known quantities and we wish to determine the friction factor (or the pressure gradient) and the torque coefficient (or the torque). The product *fRe* is given by Eq. (38), but requires prior knowledge of U_c/U whereas C_M, defined in Eq. (40), needs the ratio U_T/U_{T_i}. Note that due to the non-linear characteristic of the fluid, *fRe* and C_M are not decoupled quantities since U_c/U depends on U_T/U_{T_i} and vice-versa, as can be seen below.

To obtain these velocity ratios it is necessary to solve a system of three non-linear equations that result from the application of no-slip boundary conditions to Eqs. (23) and (25) for the axial and tangential velocities, respectively. These three equations are the cubic Eq. (26) to determine $\tilde{c}_2$, which affects both U_c/U and U_T/U_{T_i}, and the quadratic Eqs. (68) and (69) to calculate the ratios U_c/U and U_T/U_{T_i}, respectively. Note also that, even though Eq. (69) is quadratic on U_T/U_{T_i}, the determination of this quantity is straighforward.

$$
\begin{aligned}
&-\frac{1}{4}\frac{U_T}{U_{T_i}}\left(\frac{1}{y_i}-\frac{y_i}{y_o^2}\right)-\frac{\varepsilon De_{T_i}^2}{24}\left(\frac{U_T}{U_{T_i}}\right)^3\left(\frac{1}{y_i^5}-\frac{1}{y_o^6}\right)\\
&+16\varepsilon De^2\frac{U_T}{U_{T_i}}\left(\frac{U_c}{U}\right)^2 y_i\ln\kappa\\
&-16\varepsilon De^2\frac{U_T}{U_{T_i}}\left(\frac{U_c}{U}\right)^2\tilde{c}_2\left(\frac{1}{y_i}-\frac{y_i}{y_o^2}\right)\\
&-4\varepsilon De^2\frac{U_T}{U_{T_i}}\left(\frac{U_c}{U}\right)^2\tilde{c}_2^2\left(\frac{1}{y_i^3}-\frac{y_i}{y_o^4}\right)=1
\end{aligned}
\tag{68}
$$

$$
\begin{aligned}
&-\frac{1}{2}\frac{U_c}{U}(y_o^4-y_i^4)-2\tilde{c}_2\frac{U_c}{U}\left(\frac{y_i^2}{2}-\frac{y_o^2}{2}+y_o^2\ln y_o-y_i^2\ln y_i\right)\\
&+\varepsilon De_{T_i}^2\left(\frac{U_T}{U_{T_i}}\right)^2\frac{U_c}{U}\ln\frac{y_o}{y_i}\\
&-\frac{\varepsilon De_{T_i}^2}{4}\left(\frac{U_T}{U_{T_i}}\right)^2\frac{U_c}{U}\tilde{c}_2\left(\frac{1}{y_o^2}-\frac{1}{y_i^2}\right)\\
&-\frac{16}{3}\varepsilon De^2\left(\frac{U_c}{U}\right)^3(y_o^6-y_i^6)-48\varepsilon De^2\left(\frac{U_c}{U}\right)^3\tilde{c}_2(y_o^4-y_i^4)\\
&+192\varepsilon De^2\left(\frac{U_c}{U}\right)^3\tilde{c}_2^2\left(\frac{y_i^2}{2}-\frac{y_o^2}{2}+y_o^2\ln y_o-y_i^2\ln y_i\right)\\
&+64\varepsilon De^2\left(\frac{U_c}{U}\right)^3\tilde{c}_2^3\ln\frac{1}{\kappa}+\frac{\tilde{c}_3}{2}(y_o^2-y_i^2)=\frac{1+\kappa}{2(1-\kappa)}.
\end{aligned}
\tag{69}
$$

In the indirect problem, the friction factor and torque coefficient are known quantities and the aim is to determine the Reynolds and the Taylor numbers. The solution to this problem is straightforward. In fact, to determine the axial bulk velocity and angular speed it suffices to use Eqs. (31) and

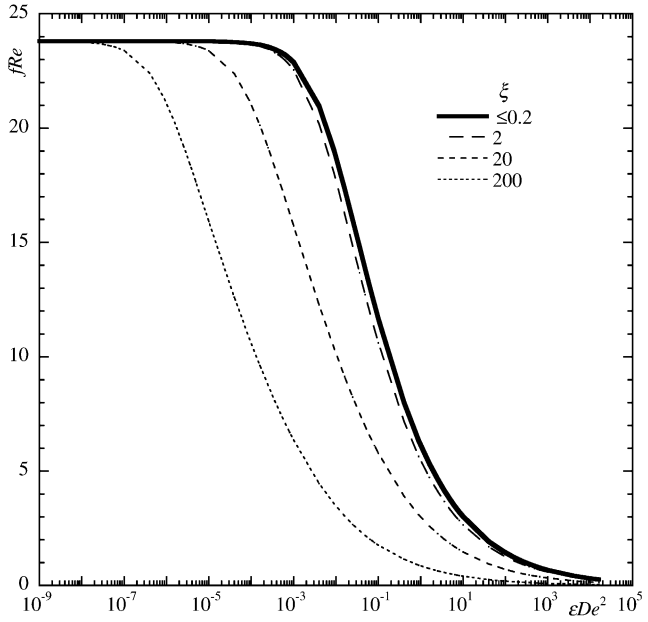

Fig. 8. Variation of fRe with ξ and εDe^2 of an SPTT fluid in annuli with $\kappa = 0.5$.

(32), respectively together with the definitions of the characteristic velocities U_c and U_T. Once U and ω are known, Re and Ta can be calculated using their definitions.

The variations of fRe and C_M with Re, Ta and εDe^2 for $\kappa = 0.5$ are shown in Figs. 8 and 9, respectively. It was found that the relevant independent quantities that determine fRe and C_M are simply εDe^2 and the velocity ratio ξ, the latter compacting the effects of both Re and Ta according to its definition ($\xi \equiv 2T/\mathrm{Re}$). For axially dominated flows ($\xi < 1$) fRe and C_M only depend on εDe^2 as represented in Figs. 8 and 9 by the curves for $\xi \leq 0.2$. The effect of εDe^2 is to decrease fRe and C_M, because the fluid shear-thins thus reducing the viscosity near the walls. The universal behaviour of C_M is due to the fact that the viscosity is defined by the axial flow and is independent of the magnitude of rotation in this range of conditions. Note also that the definition of C_M is such that it is always bounded by 1 in the Newtonian limit.

With increased rotation, the fRe versus εDe^2 curves are shifted to the left showing a decrease in friction factor for

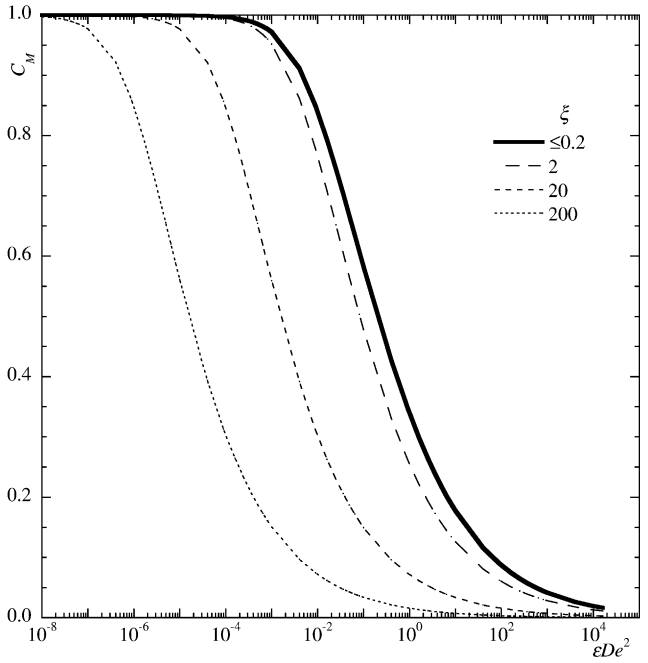

Fig. 9. Variation of C_M with ξ and εDe^2 of an SPTT fluid in annuli with $\kappa = 0.5$.

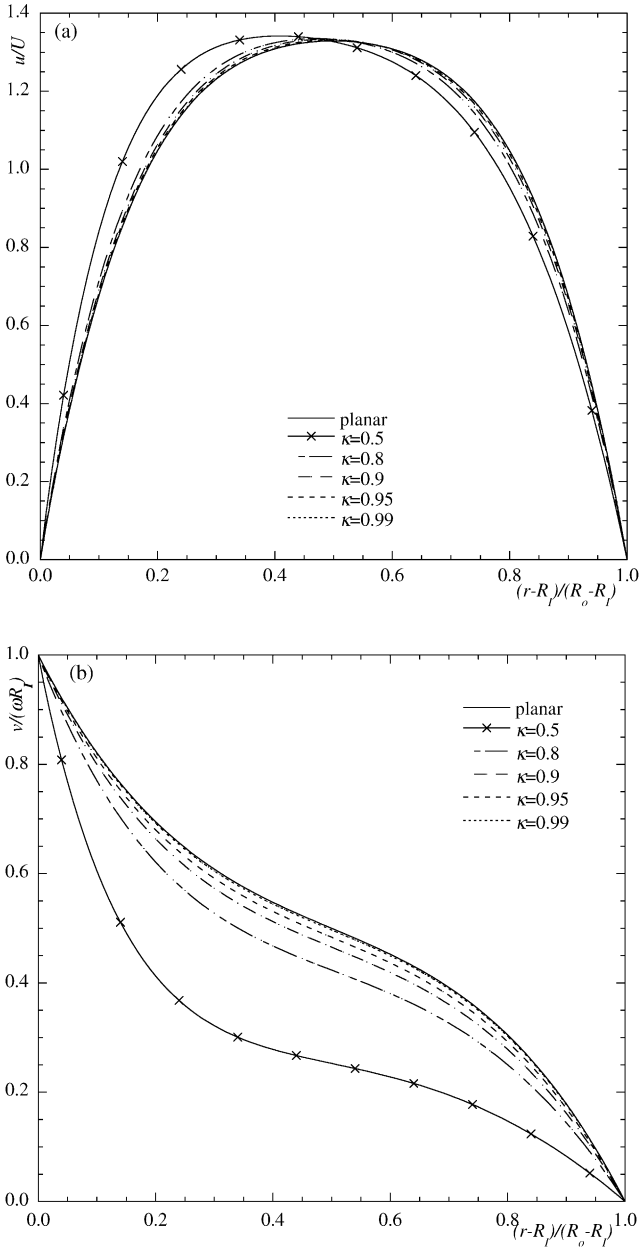

Fig. 10. Radial profiles of normalised axial (a) and tangential (b) velocities at $Re = 1$, $T = 1$ and $\varepsilon De^2 = 100$ for different radius ratios and comparison with planar solution.

the axial flow because of the decreased viscosity imparted to the shear-thinning fluid by the increasingly strong rotation. As rotation comes to dominate, the axial flow no longer determines the shear-thinning viscosity. The energy loss decreases for both axial and tangential flow and so the normalised resistance coefficients fRe and C_M decrease at identical values of the elasticity parameter εDe^2.

Although these effects take place for an elastic fluid, they are due to the inherent shear-thinning behaviour of the simplified PTT fluid and, consequently, the conclusions regarding C_M and fRe are in agreement with the observations of Escudier et al. [1] for inelastic power law fluids in concentric annuli.

4.3. Very thin annuli

For very thin annuli, the radius ratio κ approaches unity and the complex equations derived in Section 3.1 can be well approximated by the simpler expressions in Section 3.2. This is clearly shown in Fig. 10, where radial profiles of the axial and tangential velocities are plotted as a function of κ for a condition corresponding to mixed flow ($\xi = 2$) and high elasticity ($\varepsilon De^2 = 100$).

For small radius ratios the correct profiles are quite different from those for a planar geometry, especially for the azimuthal velocity component, but approach the planar solution as $\kappa \to 1$. In the particular flow condition of the figure, the axial velocity profile at $\kappa = 0.9$ is already close to the simpler planar profile, whereas for the tangential velocity the difference is still remarkable and it is necessary to attain $\kappa = 0.99$ to have negligible differences. The impact on integral quantities reflect the effect on the corresponding relevant velocity profiles.

5. Conclusions

Analytical solutions have been derived for the skewed Poiseuille–Couette flows of nonlinear viscoelastic PTT fluids in concentric annuli and planar channels. These flows are formed by the combination of an imposed constant pressure gradient in the axial/longitudinal direction and the movement of a wall in a normal direction, namely the rotation of the inner cylinder or the spanwise motion of a plate. Expressions are presented for the radial variation of the axial and tangential velocities, as well as for the three shear stresses and the two normal stresses (transverse variation of the longitudinal and spanwise velocities in the planar case).

For the axisymmetric flow it was found that under conditions of axial dominated flow the peak axial velocity is in the center of the annulus and becomes plug like as εDe^2 increases, while the tangential velocity progressively distorts to a sigmoidal shape. The tangential shear stress, that balances the applied torque, has always a universal behavior and the axial shear stress, balancing the axial pressure gradient, has a quasi-universal variation with εDe^2. In contrast, for rotation dominated flows the tangential velocities always have a monotonic variation and the flow is distorted towards the inner cylinder where viscosities are lower. Now, the axial shear stress shows a clear dependence on fluid elasticity.

For engineering purposes expressions were also derived relating the friction factor and torque coefficient to the Reynolds number, Taylor number, εDe^2 (quantifying flow elasticity) and the radius ratio. When the flow is axially dominated, fRe and C_M only depend on εDe^2 for a given annulus, but they decrease with the velocity ratio as rotation increases in strength. In all cases, an increase in flow elasticity leads to a reduction in the axial and rotational resistance to the flow. Regarding fRe and C_M it was found that the velocity ratio adequately compacts the effects of both the Reynolds number and the Taylor number.

As the annulus thins ($\kappa \to 1$) the flow field approaches that given by the solution for the skewed planar Poiseuille–Couette flow which is given by the simpler equations of Section 3.2.

Acknowledgements

The authors wish to thank CNPq of Brasil and ICCTI of Portugal for funding this work with the exchange programme Project 2001 Proc C 4.3.1 in 2002.

References

[1] M.P. Escudier, P.J. Oliveira, F.T. Pinho, Fully developed laminar flow of purely viscous non-Newtonian liquids through annuli including the effects of eccentricity and inner-cylinder rotation, Int. J. Heat Fluid Flow 23 (2002) 52–73.
[2] R.K. Bhatnagar, Steady laminar flow of visco-elastic fluid through a pipe and through an annulus with suction or injection at the walls, J. Ind. Inst. Sci. 45 (1963) 126–151.
[3] A.C. Dierckes, W.R. Schowalter, Helical flow of a non-Newtonian polyisobutelene solution, Ind. Eng. Chem. Fund. 5 (2) (1966) 263–271.
[4] P.N. Kaloni, On the helical flow of an elasto-viscous fluid, Ind. J. Pure Appl. Phys. 3 (1965) 1–3.
[5] P.K. Kulshrestha, Helical Flow of an Idealized Elastico-Viscous Liquid (I)*, ZAMP XIII, (1962), pp. 553–561.
[6] F.T. Pinho, P.J. Oliveira, Axial annular flow of a non-linear viscoelastic fluid—an analytical solution, J. Non-Newt. Fluid Mech. 93 (2000) 325–337.
[7] A.N. Beris, R.C. Armstrong, R.A. Brown, Perturbation theory for viscoelastic fluids between eccentric rotating cylinders, J. Non-Newt. Fluid Mech. 13 (1983) 109–143.
[8] R.B. Bird, R.C. Armstrong, O. Hassager, Dynamics of Polymeric Liquids. Fluid Mechanics, second ed., vol. I. Wiley, 1987, p. 314 and 387.
[9] B.D. Coleman, H. Markowitz, W. Noll, Viscometric Flows of Non-Newtonian Fluids, Springer-Verlag, Berlin, 1966.
[10] H.W. Giesekus, Die sekundarströmung in einer Kegel–Platte–Anordnung: Abhängigkeit von der Rotationsgeschwindigskeit bei verschiedene Polymersystemen, Rheol. Acta 6 (1967) 339–353.
[11] K. Walters, N. Waters, On the use of a rheogoniometer. Part 1. Steady shear, in: R. Wetten, R. Whorlow (Eds.), Polymer Systems—Deformation and Flow, Macmillan, London, 1968, pp. 211–235.

[12] J.J. Joseph, Slow motion and viscometric motion stability and bifurcation of the rest state of a simple fluid, Arch. Rat. Mech. Anal. 56 (1974) 99–157.
[13] C.T. Hill, Nearly viscometric flow of viscoelastic fluids in the disk and cylinder system. II. Experimental, Trans. Soc. Rheol. 16 (1972) 213–245.
[14] B. Debbaut, B. Hocq, On the numerical simulation of axisymmetric swirling flows of differential viscoelastic liquids: the rod climbing effect and the Quelleffekt, J. Non-Newt. Fluid Mech. 43 (1992) 103–126.
[15] J.J. Joseph, Fluid Dynamics of Viscoelastic Liquids. Applied Mathematical Science Series No. 84, Springer-Verlag, Berlin, 1990, pp. 510–514.
[16] J.M. Nouri, H. Umur, J.H. Whitelaw, Flow of Newtonian and non-Newtonian fluids in concentric and eccentric annuli, J. Fluid Mech. 253 (1993) 617–641.
[17] M.P. Escudier, I.W. Gouldson, D.M. Jones, Flow of shear-thinning fluids in a concentric annulus, Exp. Fluids 18 (1995) 225–238.
[18] S.H. Hashemabadi, S.Gh. Etemad, J. Thibault, M.R. Golkar-Naranji, Analytical solution for dynamic pressurization of viscoelastic fluids, Int. J. Heat Fluid Flow 24 (2003) 137–144.
[19] N. Phan-Thien, R.I. Tanner, A new constitutive equation derived from network theory, J. Non-Newt. Fluid Mech. 2 (1977) 353–365.
[20] J. Azaiez, R. Guénette, A. Aït-Kadi, Numerical simulation of viscoelastic flows through a planar contraction, J. Non-Newt. Fluid Mech. 62 (1996) 253–277.
[21] M.M. Alves, F.T. Pinho, P.J. Oliveira, Study of steady pipe and channel flows of a single-mode Phan–Thien–Tanner fluid, J. Non-Newt. Fluid Mech. 101 (2001) 55–76.
[22] R. Keunings, M.J. Crochet, Numerical simulation of the flow of a viscoelastic fluid through an abrupt contraction, J. Non-Newt. Fluid Mech. 14 (1984) 279–299.
[23] C. Nouar, C. Desaubry, H. Zenaidi, Numerical and experimental investigation of thermal convection for a thermodependent Herschel–Bulkley fluid in an annular duct with rotating inner cylinder, Eur. J. Mech. B 17 (1998) 875–900.
[24] M.P. Escudier, P.J. Oliveira, F.T. Pinho, S. Smith, Fully developed laminar flow of non-Newtonian liquids through annuli: comparison of numerical calculations with experiments, Exp. Fluids 33 (2002) 101–111.
[25] R.C. Di Prima, H.L. Swinney, Instabilities and transition in flow between concentric rotating cylinders, in: H.L. Swinney, J.P. Gollub (Eds.), Hydrodynamic Instabilities and the Transition to Turbulence, Springer, 1981, pp. 139–180.